Different Bone Integration Profiles of Turned and Acid-etched Implants Associated with Modulated Expression of Extracellular Matrix Genes

Takahiro Ogawa, DDS, PhD[1]/Ichiro Nishimura, DDS, DMD, DMSc[2]

Purpose: *The manner in which surface roughness of implants affects bone-implant integration remains unknown. This study correlated morphologic profiles of bone-implant integration and extracellular matrix (ECM) gene expression in response to the placement of implants with different surface topographies.* ***Materials and Methods:*** *T-shaped hollow implants with turned and dual acid-etched (DE) surfaces were placed into rat femurs. A bone integration curve (BIC) was created from serial histomorphometric measurements within the implant chamber. The mRNA expression pattern of ECM genes in bone healing with or without implants was examined using reverse transcriptase-polymerase chain reaction.* ***Results:*** *At week 2, the BIC of the DE implant increased near the implant surface, whereas that of the turned implant decreased. The bone-to-implant contact rate of the DE implant was 6- and 2.5-fold higher than that of the tuned implant at weeks 2 and 4, respectively. A spatially standardized histomorphometry revealed that, at week 2, the DE implant had a greater bone volume than the turned implant in a zone near the implant, but not in zones distant from the implant surface. The DE implant evoked an accelerated mRNA expression for osteonectin and osteocalcin compared with the turned implant, along with an up-regulated expression for bone sialoprotein II, collagen III, and integrins in initial healing stages up to week 1.* ***Discussion and Conclusion:*** *The results indicate that different histologic bone integration profiles associated with increased surface roughness may be explained, in part, by the modulated expression of the selected ECM-related genes. The data provide evidence supporting the fact that gene regulation occurs at local levels of implant surfaces in vivo.*
(Int J Oral Maxillofac Implants 2003;18:200–210)

Key words: *dental implants, extracellular matrix, histomorphometry, osseointegration, titanium*

Bone wound healing around endosseous implants has been characterized as unique osteogenesis embodying an amorphous interfacial layer and contiguous bone formation spreading along the implant surface.[1,2] Increased roughness of implant surfaces reportedly induces increased mechanical fixation of implants.[3,4] Whereas a simple mechanical interlocking may occur in the roughened surface, increased cell-binding protein adsorption on rougher surfaces may increase osteoblastic cellular attachment.[5,6] The latter phenomenon may result in a proportional increase of bone matrix production and bone volume. It has also been postulated that cellular function and surface topography of implants are directly interrelated.[7,8]

Whether and how the surface topography of implants affects the histologic profile of bone is still controversial. Variations in surface roughness experimentally created by chemical and/or mechanical methods have not been clearly associated with the histologic evidence of increased or decreased implant-related osteogenesis.[9–11] Bone healing around implants has been described as a combination of events of bone formation along the implant

[1]Assistant Professor, The Jane and Jerry Weintraub Center for Reconstructive Biotechnology, Division of Advanced Prosthodontics, Biomaterials and Hospital Dentistry, UCLA School of Dentistry, Los Angeles, California.
[2]Professor, The Jane and Jerry Weintraub Center for Reconstructive Biotechnology, Division of Advanced Prosthodontics, Biomaterials and Hospital Dentistry, UCLA School of Dentistry, Los Angeles, California.

Reprint requests: Dr Takahiro Ogawa, The Jane and Jerry Weintraub Center for Reconstructive Biotechnology, Division of Advanced Prosthodontics, Biomaterials and Hospital Dentistry, UCLA School of Dentistry, Box 951668, CHS B3-087, Los Angeles, CA 90095-1668. Fax: +310-825-6345. E-mail: tack@dent.ucla.edu

surface and stimulated wound healing and remodeling of surrounding tissues.[12,13] Therefore, the effect of the surface topography on the implant-related osteogenesis should be examined separately in different zones relative to the distance from the implant surface. However, conventional experimental models using an analog dental implant design exhibit an inherent challenge in differentiating these zones as well as in discriminating the newly formed bone from modeled and remodeled bone around the implant.

The hypothesis to be tested was that the gene expression is controlled at local levels of implant surfaces, which may, in part, explain different histologic bone formation profiles on different surface topographies. A T-shaped hollow experimental implant was fabricated that allowed ingrowth of the implant-induced de novo tissue for histomorphometric and molecular analyses. Reported here is the in vivo modulation of bone extracellular matrix (ECM) gene expression in response to the placement of titanium implants with 2 different surface topographies: turned and dual acid-etched.

MATERIALS AND METHODS

Implant Design and Surface Analyses

Experimental T-shaped implants were fabricated from commercially pure titanium and had a hollow inner chamber (3.0×3.0×0.8 mm) (Fig 1a). The implant surface was either turned by machining or treated by dual acid-etching (DE) (Osseotite, Implant Innovations, Palm Beach Gardens, FL). Both surfaces were prepared by Implant Innovations. The surface of the implants was examined by scanning electron microscopy (SEM) (Stereoscan 250, Cambridge Instruments, Cambridge, United Kingdom) and atomic force microscopy (AFM) (Park Scientific Instruments, Sunnyvale, CA). Packaged algorithm software combined with AFM produced the values of peak-to-valley (Rp-v), root mean square roughness (Rrms), and average roughness (Ra). The measurement was made at 3 sites on the sidewall of the inner chamber, and average values were calculated.

Surgery

For histologic analyses, twelve 8-week-old male Sprague-Dawley rats were employed. The implants were cleaned with 70% ethanol and sterilized by autoclaving. Rats were anesthetized with a 1% to 2% isoflurane inhalation. After the leg was shaved and decontaminated with 10% povidone-iodine solution, the distal aspect of the femur was carefully exposed. The flat surface of the distal femur was selected for implant placement. The implant site was prepared by drilling at 7 mm from the distal edge of the femur (Fig 1b). Irrigation with sterilized isotonic saline solution was used for cooling and cleaning. The implant was placed into the site until the implant roof structure reached the femur exterior, and stability was confirmed with a mechanical fit. Six rats received the turned implant, and the remaining 6 rats received the DE implant. Muscle and skin openings were closed separately.

For molecular analyses 39 rats were used. Twenty-four rats were placed with either the turned or DE implant as above. Controls were treated as follows:

- A non-implant defect with a size and depth same as the implant dimensions was created at the corresponding site of 12 rats.
- The remaining 3 rats received no surgical treatment.

This study protocol was approved by the University of California at Los Angeles Chancellor's Animal Research Committee.

Histologic Procedure and Histomorphometric Analysis

Three rats each were sacrificed at each 2- and 4-week period post-operation for both turned and DE implant groups, and then were perfused through the abdominal aorta with a solution of 4% formaldehyde and 2% glutaraldehyde. Next, the femur was harvested and further fixed in 10% buffered formalin for 2 weeks at 4°C. The specimens were dehydrated in an ascending series of alcohol rinses and embedded in light-curing epoxy resin (Technovit 7200 VLC, Hereaus Kulzer, Wehrheim, Germany) without decalcification. The embedded specimens were sawed perpendicular to the exposed implant roof structure at a site 1 mm from the medial end of the implant, which produced cross sections parallel to the inner chamber opening (Fig 1c). The specimens were ground to a thickness of 30 μm with a grinding system (Exakt Apparatebau, Norderstedt, Germany). The sections were stained with Goldner's trichrome stain and observed with a light microscope.

A 20× magnification lens and 2× zoom on a computer display were used for computer-based histomorphometric measurements (Image Pro-plus, Media Cybernetics, Silver Spring, MD). To identify the details of the tissue structure, microscopic magnification up to 100× was used. In an attempt to determine the bone-implant integration curve (BIC), configuration of the bone tissue associated

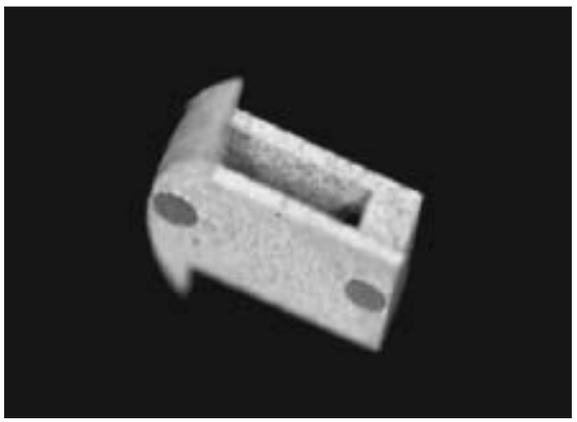

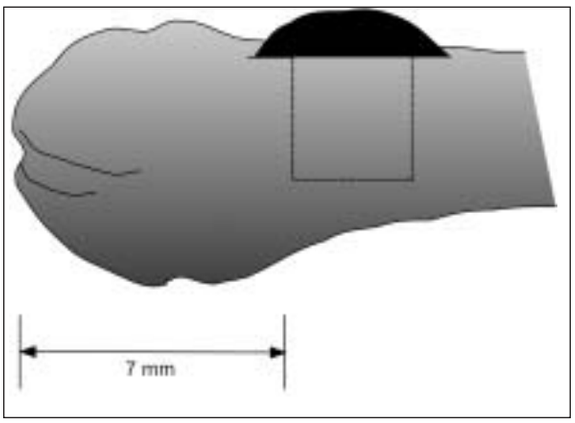

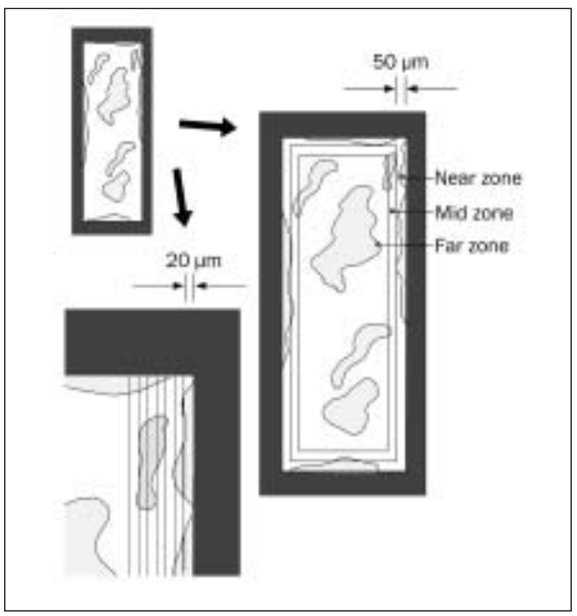

Fig 1a *(Above left)* T-shaped implant, which has a roof structure and inner chamber.

Fig 1b *(Above right)* Schematic description of the implant site. The implant is placed at a consistent site in the distal end of the femur and is incorporated inside the bone up to the roof structure level.

Fig 1c *(Left)* Schematic description of histologic cross section and histomorphometric analyses. The solid black area represents the implant structure, and the shadowed area represents bone tissue. To create a bone integration curve, the length of the lines located within the bone tissue *(thick lines)* was summed at each vicinity level from the implant surface, from the 20-µm level up to 300 µm, at 20-µm intervals *(lower left).* To measure the bone volume in the spatially standardized areas, the tissue area was divided into 3 areas: near, mid, and far zones from the surface of the implant *(right).* The near zone is defined as a circumferential area contiguously located along the implant surface with a width of 50 µm. The mid zone is defined as an area next to the near zone with a width of 50 µm. The far zone is the rest of the chamber.

with the levels of vicinity to the implant surface was examined. In detail, fifteen lines were drawn parallel with the long axis of the chamber at every 20 µm up to 300 µm from the implant surface (Fig 1c). The length of the lines within the bone tissue were summed. The sum divided by the entire length of the line was defined as the bone rate (%). The data were plotted as line graphs to create the BIC.

Bone volume measurements in the spatially standardized area were obtained by dividing the implant chamber into 3 zones as follows (Fig 1c):

- Near zone, the circumferential zone within 50 µm of the implant surface
- Far zone, the zone greater than 100 µm from the surface
- Mid zone, the zone between the near and far zones

The following variables were analyzed:

- Bone-implant contact rate (%) = (sum of the length of bone-implant contact)/(circumference of the inner chamber) × 100
- Bone volume in near zone (%) = (bone area in near zone)/(area of near zone) × 100
- Bone volume in mid zone (%) = (bone area in mid zone)/(area of mid zone) × 100
- Bone volume in far zone (%) = (bone area in far zone)/(area of far zone) × 100
- Total bone volume (%) = (bone area in the chamber)/(area of the chamber) × 100

The implant-bone contact was defined as the interface where bone tissue was located within 10 µm of the implant surface without any intervention of soft tissue.

Table 1 Primer Sequence and Amplification Condition for Polymerase Chain Reaction (PCR)

	Forward primer	Backward primer	Annealing temperature	No. of cycle	Size of PCR products (bp)
Collagen I	5′-GGCAACAGTCGATTCACC-3′	5′-AGGGCCAATGTCCATTCCG-3′	59°C	19	177
Collagen III	5′-CCTGGACCTCAGGGTATC-3′	5′-TGCAGGGCCTGGACTACC-3′	60°C	25	498
BSPII	5′-CAGGAGGCGGAGGCAGAG-3′	5′-CATACTCAACCGTGCTGC-3′	63°C	25	487
Osteonectin	5′-GCCAGGACCCCACCAGCT-3′	5′-CGGGTGCTGATCCAGCTG-3′	60°C	21	380
Osteopontin	5′-GATTATAGTGACACAGAC-3′	5′-AGCAGGAATACTAACTGC-3′	45°C	19	443
Osteocalcin	5′-GTCCCACACAGCAACTCG-3′	5′-CCAAAGCTGAAGCTGCCG-3′	60°C	19	193
Integrin beta 1	5′-GCAGTTTGTGGGTCGCTG-3′	5′-GCCCACTGCTGACTTAGG-3′	63°C	24	544
Integrin beta 3	5′-GGCTGGAGGAATGATGCA-3′	5′-GCTCTTCGGGGAGATCAC-3′	61°C	25	388

BSP = bone sialoprotein.

Gene Expression Analysis

The animals in the turned implant and the DE implant groups were divided into 4 groups of 3 each and sacrificed at day 3 and weeks 1, 2, and 4 of the healing period. Implants containing tissues that had grown inside the inner chamber were harvested, and total RNA was isolated using a phenol-ethanol precipitation method that employed a TRIzol reagent (Life Technologies, Gaithersburg, MD). Tissue was also extracted from the non-implant defect groups at day 3 and weeks 1, 2, and 4 and from the untreated controls at week 2.

Reverse transcriptase–polymerase chain reaction (RT-PCR) assay was used to analyze the expression of ECM-related genes. Following DNase I treatment, 1 μg of total RNA was reverse-transcribed into a cDNA template using MMLV reverse transcriptase (Clontech, Palo Alto, CA) and oligo(dT) primer (Clontech) at 42°C for 1 hour, followed by 94°C for 5 minutes. The cDNA products were amplified by PCR using Taq DNA polymerase (Amersham Pharmacia Biotech, Piscataway, NJ) for the following ECM-related genes: alpha 1 type I collagen, alpha 1 type III collagen, osteopontin, osteocalcin, osteonectin, bone sialoprotein II (BSPII), integrin beta-1 subunit, and integrin beta-3 subunit. Specific custom oligo-primers were designed based on the rat mRNA sequence of each protein, as shown in Table 1.

Preliminary PCR trials were performed to determine the annealing temperature and the optimal number of cycles that yields the linear range of PCR amplification for each primer set (Table 1). Cycle parameters were as follows: primer-specific number of cycles of 94°C for 1 minute, primer-specific annealing temperature for 1 minute, 72°C for 2 minutes, followed by an extension of 72°C for 10 minutes in the final cycle. The PCR products were visualized on 1.5% agarose gel with ethidium bromide staining. The intensity of the bands was quantified under ultraviolet light (Eagle Eye II, Stratagene, La Jolla, CA) and normalized with respect to those for GAPDH (housekeeping gene) mRNA. To create the time course of the gene expression level, the calculated values of each band relative to GAPDH were standardized with respect to the untreated femur bone control. Identification of PCR products was confirmed through cloning and sequencing of the bands. The PCR products were subcloned into pCRII vector of the TA cloning kit (Invitrogen, San Diego, CA). The transformed plasmids containing an insert of a correct size were sequenced using T7 primer.

Statistical Methods

A 2-way analysis of variance (ANOVA) at $P < .05$ level of significance was applied to determine the effect of the length of the healing period and different surface topography on the histomorphometric variables. At each healing period, the variables of the turned and DE implants were compared by the Mann-Whitney *U* test. The Mann-Whitney *U* test was also used to examine the difference between weeks 2 and 4.

RESULTS

Surface Topography of Implants

SEM analysis of the turned implant showed isotropic marks oriented perpendicular to the long axis of the implant (Fig 2a), whereas the DE implant exhibited irregular but consistent surface roughness (Fig 2b). AFM images showed that the turned surface was slightly wavy and flat (Fig 2c), whereas the DE surface appeared bumpy (Fig 2d). AFM calculations were Rp-v = 0.51 μm, Rrms = 0.079 μm, and Ra = 0.063 μm for the turned

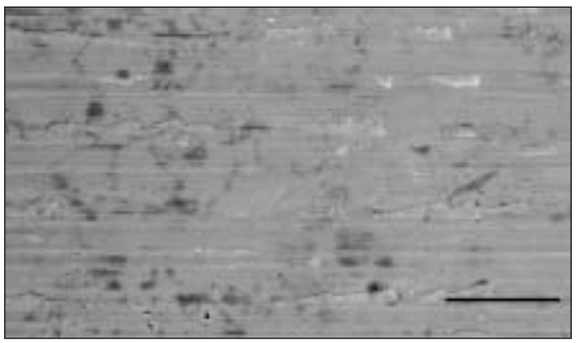

Fig 2a SEM image of turned implant depicting isotropic marks perpendicular to the long axis of the implant. Bar = 10 μm.

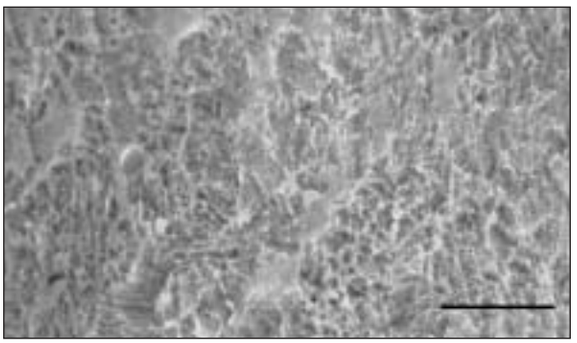

Fig 2b SEM image of the DE implant with non-directional roughness. Bar = 10 μm.

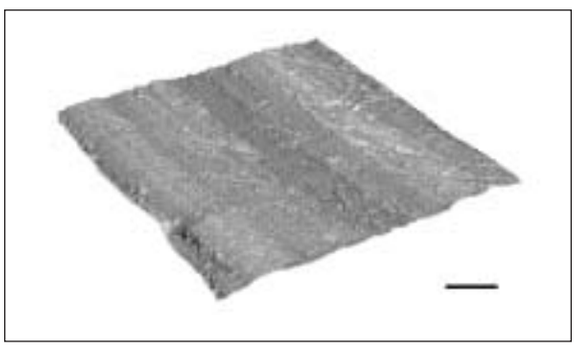

Fig 2c AFM image of the turned implant surface. A slightly wavy and flat surface is shown. Bar = 1 μm.

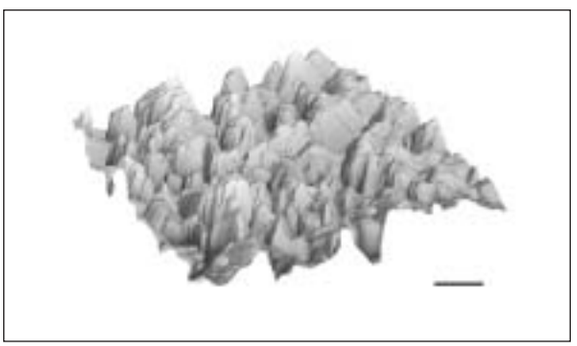

Fig 2d AFM image of the DE implant surface. A 3-dimensionally rougher surface than the turned surface is apparent. Bar = 1 μm.

implant and Rp-v = 1.17 μm, Rrms = 0.198 μm, and Ra = 0.159 μm for the DE implant.

Histologic Observations

At week 2, bone tissue or bonelike tissue with a woven, immature appearance had formed within the inner chamber and along the implant surface of both the turned and DE implants (Figs 3a to 3d). Direct contact of the bone with the implant surface was rarely observed for the turned implant, and connective tissue was interposed between the bone and the implant. In the DE implant, the bone tissue was spread along the implant surface, and some bone tissue was directly in contact with the implant surface without soft tissue intervention.

At week 4 the trabecular structure of bone tissue dramatically decreased, and the middle of the chamber was filled with fatty bone marrow consisting of hematopoietic tissue. The bone tissue with the lamellar structure extensively encapsulated both turned and DE surfaces. However, the turned implant still exhibited fibrous connective tissue intervening between the bone tissue and the implant surface. In contrast, the DE surface showed an extensive area with a bone tissue layer without connective tissue intervention.

Histomorphometric Observations

The BIC portrayed variable bone configuration according to the healing time and the surface topography (Figs 4a to 4d). The BIC of the turned implant at week 2 was described by a constant bone rate from the middle of the chamber up to the nearby level of the implant surface, followed by a drop at the 20-μm level. The BIC of the DE implant exhibited an increased bone rate at the 40-μm level. Unlike the turned implant, the DE implant did not show a bone rate drop at the 20-μm level compared with its baseline level. The BIC at week 4 consisted of a remarkable increase in bone rate toward the nearby area of the implant surface for both turned and DE implants. The increase in bone rate of the turned implant plateaued at the 40-μm level. The bone rate of the DE implant reached a sharp peak over 80% at the 20-μm level.

The 2-way ANOVA indicated that the bone-to-implant contact rate was significantly affected by both the healing time (P = .0012) and the surface topography (P = .0041) (Fig 5a). However, the effect of the interaction of healing time and surface topography on the bone-implant contact rate was insignificant (P = .103). The Mann-Whitney test

revealed that the bone-implant contact rate increased significantly from weeks 2 to 4 for both turned and DE implants (P = .0495). The Mann-Whitney test also indicated a greater bone-to-implant contact rate for the DE implant than for the turned implant (6-fold at week 2 and 2.5-fold at week 4; P = .0495).

The bone volume in the near zone was significantly influenced by the healing time (2-way ANOVA, P = .0084) but not by the surface topography (P = .5907) or the interaction of the healing time and surface topography (P = .0780) (Fig 5b). The bone volume in the near zone increased significantly from weeks 2 to 4 for the turned implant (Mann-Whitney, P = .0495) but not for the DE implant (P = .5127). The DE implant showed over 2-fold greater bone volume than the turned implant at week 2 (Mann-Whitney, P = .0495), while there was no significant difference between them at week 4.

The effect of the healing time (2-way ANOVA, P = .8782), the surface topography (P = .3477), and the interaction of the healing time and surface topography on bone volume in the mid zone (P = .8420) was insignificant (Fig 5c). Bone volume in the mid zone did not differ between weeks 2 and 4 or between the turned and DE implants ($P > .05$).

The far zone bone volume decreased over time (2-way ANOVA, P = .0015), whereas the surface topography (P = .2035) and the interaction of healing time and surface topography (P = .1720) did not affect the bone volume (Fig 5d). The bone volume with the turned implant decreased significantly from week 2 to week 4 (Mann-Whitney, P = .0495). The change trend for the DE implant was not significant (P = .1266). No difference was found between the turned and DE implants at weeks 2 (P = .1266) or 4 (P = .8273).

The total bone volume was not influenced by the healing period (2-way ANOVA, P = .1394), surface topography (P = .1498), or the interaction of the healing period and surface topography (P = .9023) (Fig 5e). The Mann-Whitney test also showed no healing time–dependent or surface topography–dependent difference ($P > .05$).

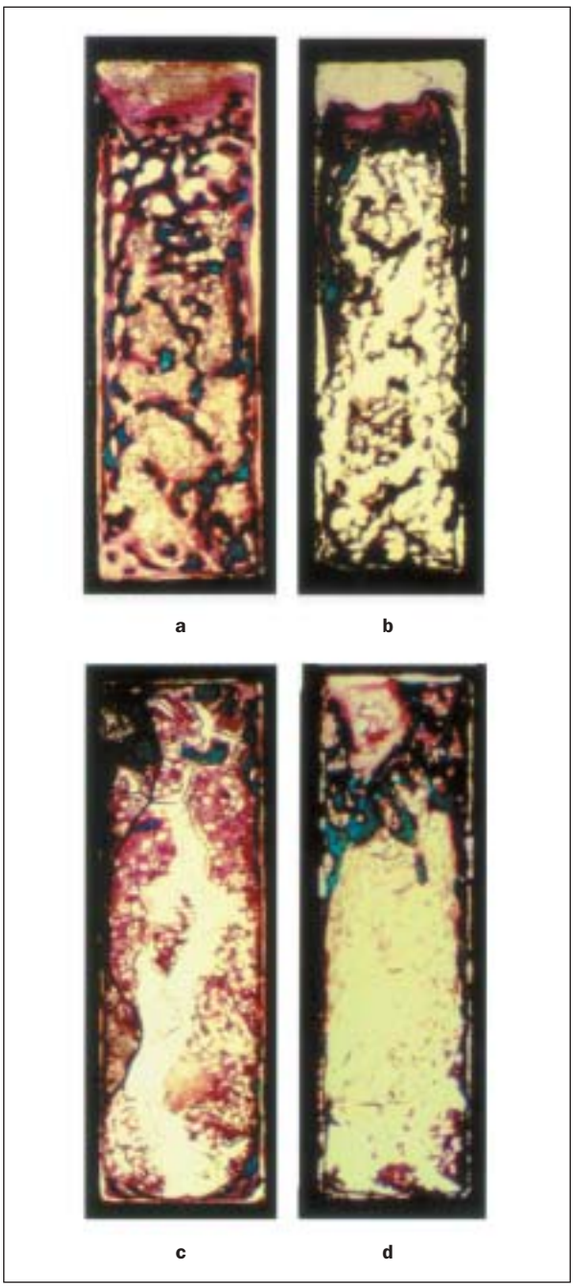

Figs 3a to 3d Histologic sections of *(above left)* the turned implant at week 2, *(above right)* the DE implant at week 2, *(below left)* the turned implant at week 4, and *(below right)* the DE implant at week 4.

Bone Matrix Gene Expression

The mRNA expression time course was determined for all of the ECM molecules (Figs 6a and 6b). The expressions patterns of osteonectin and osteocalcin were characterized by a rapid up-regulation for the DE implant together with a delayed up-regulation for the turned implants compared with the non-implant defect. The expression of the DE implant peaked at week 1, while that of the turned implant peaked at week 2. These genes showed a 2-phase expression pattern of the non-implant defect with a depression at week 1. An up-regulated expression for the DE implant over the non-implant defect at an early healing stage of week 1 was also seen for BSPII, collagen III, and integrins beta 1 and beta 3. After week 1, the expression level of all of the tested genes tended to decline rapidly for the DE implant compared with the turned implant. The turned

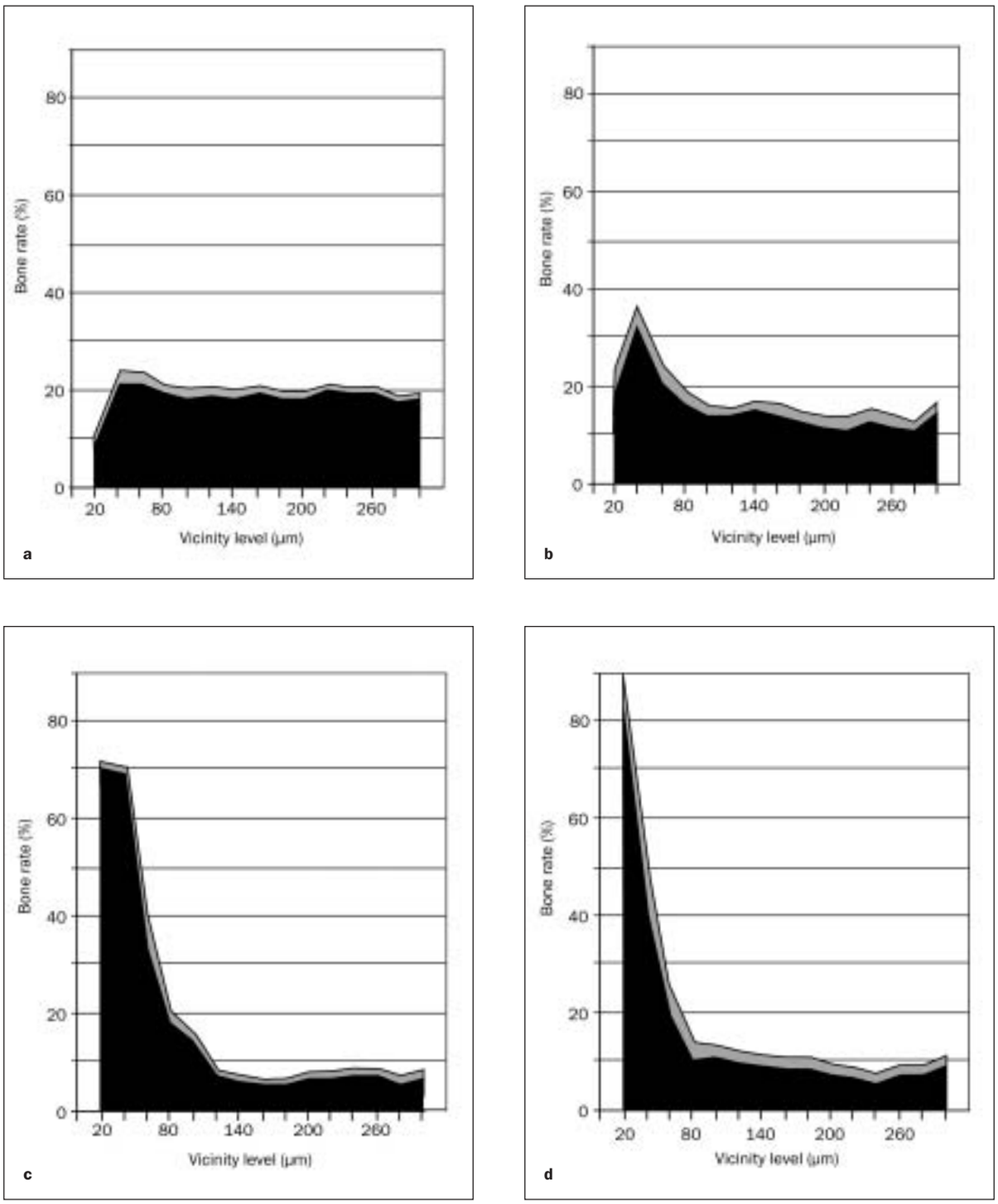

Figs 4a to 4d Bone integration curves of (a) the turned implant at week 2, (b) the DE implant at week 2, (c) the turned implant at week 4, and (d) the DE implant at week 4. The average bone rate *(solid black)* and standard error *(gray)* are plotted at intervals of every 20 µm beginning from the implant surfaces.

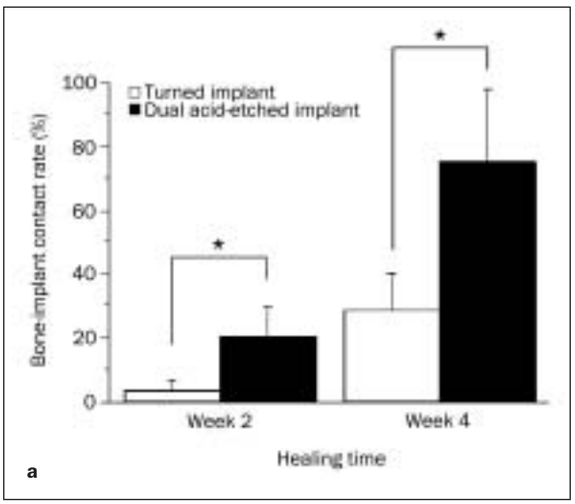

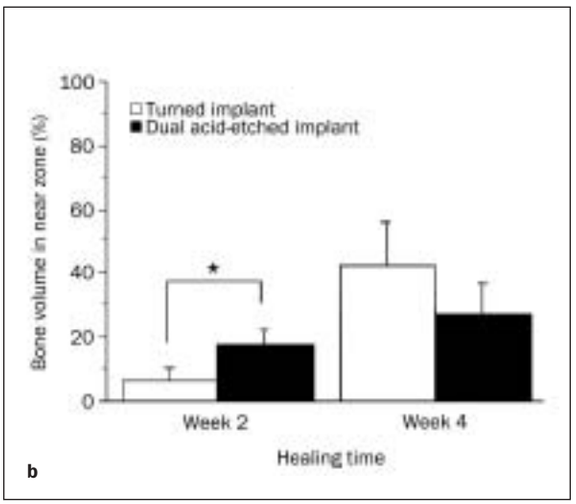

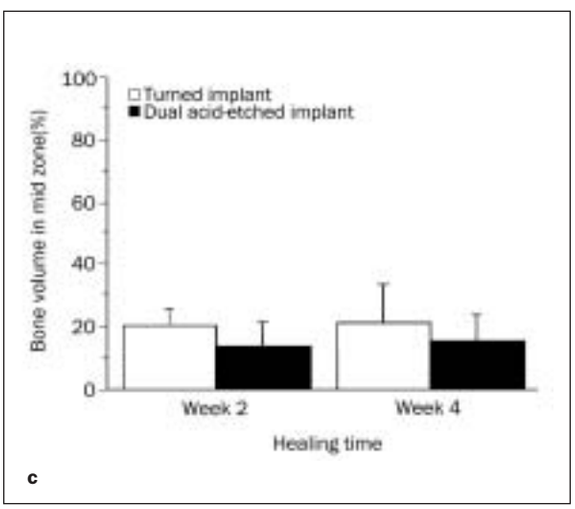

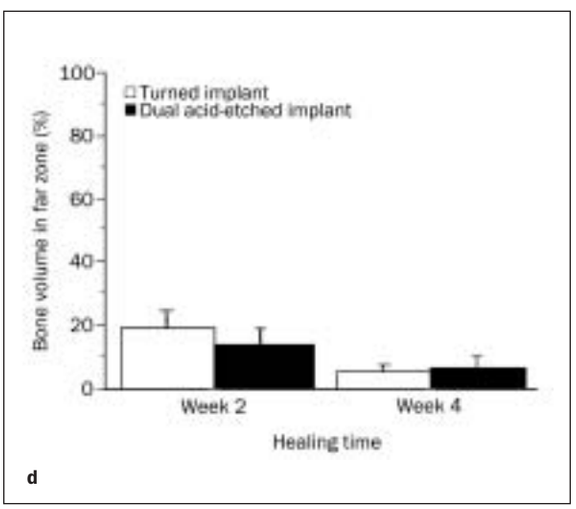

Figs 5a to 5e The average histomorphometric values with standard deviation (error bars) of bone-implant contact rate (a), bone volume in the near zone (b), bone volume in the mid zone (c), bone volume in the far zone (d), and total bone volume (e). Asterisk = significant differences ($P < .05$) between turned and DE implants as determined by the Mann-Whitney *U* test.

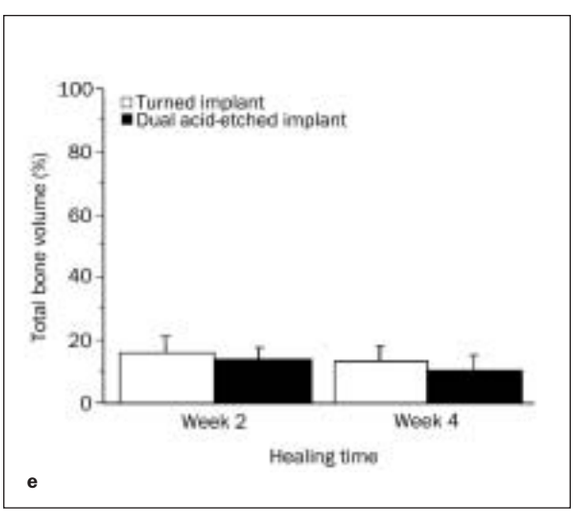

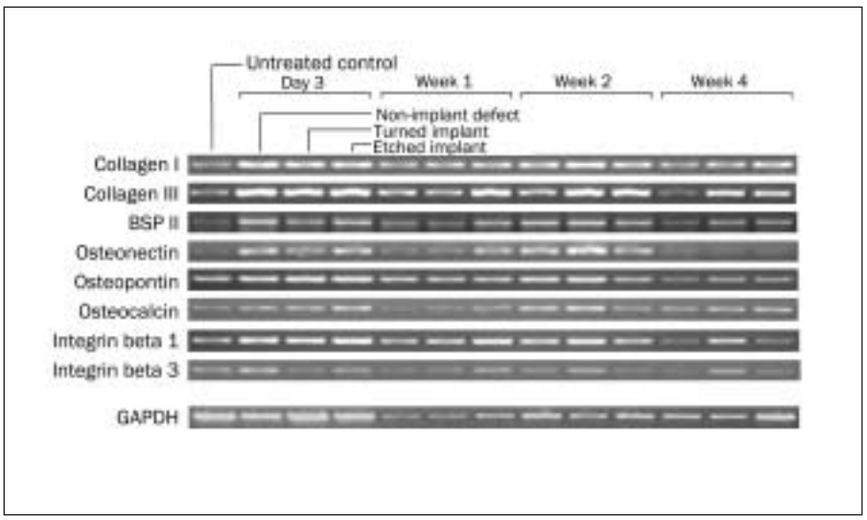

Fig 6a Expression of the bone ECM-related mRNA and GAPDH represented by reverse transcriptase–polymerase chain reaction at day 3 and weeks 1, 2, and 4 of healing time.

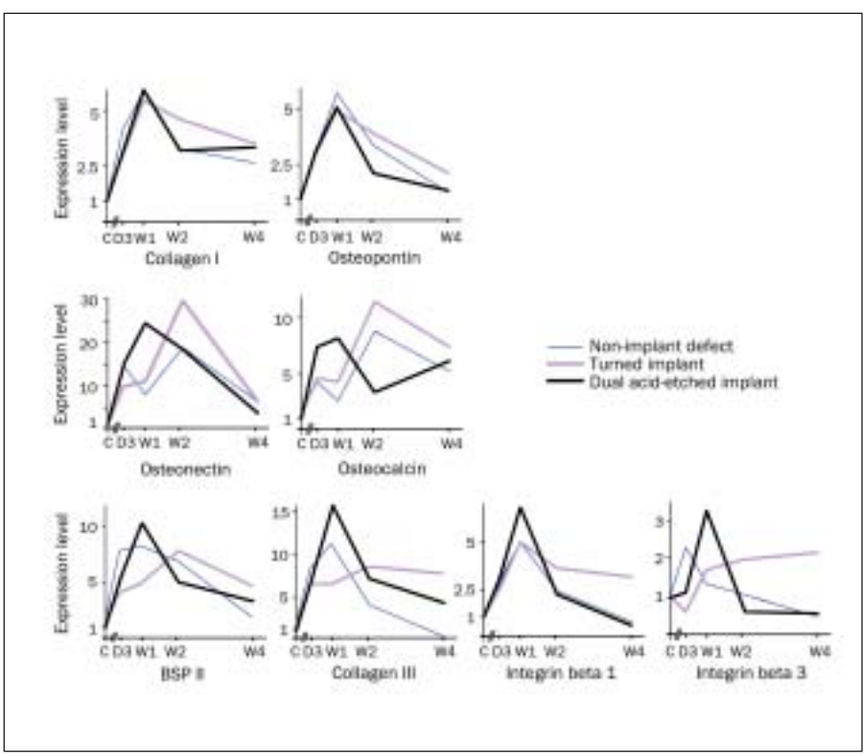

Fig 6b Expression time course of the bone matrix mRNA. The relative intensity of each band was calculated in relation to that of GAPDH. Further, the relative intensities were normalized relative to that of the untreated control to obtain the final values of expression level (arbitrary unit) (y-axis).

implant did not show an early stage expression peak (within week 1) for osteonectin, osteocalcin, BSPII, collagen III, and integrin beta 3. Instead, the expression level of integrins beta 1 and beta 3 for the turned implant was sustained up to week 4.

DISCUSSION

The BIC illustrated the differences in bone configuration between the turned and DE implants at the surface-nearby area (near zone). The statistical analyses demonstrated that the DE implant exhibited an increased bone-implant contact rate throughout the healing period and increased bone volume in the near zone at the early healing stage. Analyses of bone volume in the mid and far zones did not yield any significant difference between the turned and DE implants. Also, the comparisons in bone volume at each near, mid, and far zone between weeks 2 and 4 characterized the osteogenic pattern around implants as a thin layer of bone but with less resorption or remodeling, which was distinct from the osteogenic pattern occurring in the distant area. These results indicated that histologic profiles in only the near zone were affected by the placement of implants and their surface topography and that the mid and far zones may simply represent the bone healing and remodeling after ablation surgery regardless of the placement of implants. In this context, the differential expression patterns of the tested ECM-related genes between the defect and implant samples may reflect phenotypic alteration occurring in the near zone in response to the implants.

The fluctuating expression pattern in response to the implant placement and surface topography varied among the genes tested. In terms of the effect of the surface topography, the DE surface evoked an up-regulated expression of the selected genes at the initial healing stage of week 1, compared with the non-implant defect (osteonectin, osteocalcin, BSPII, collagen III, and integrins beta 1 and beta 3). Expression of these genes around the turned surface was either delayed (osteonectin, osteocalcin) or sustained without typical early stage expression peak (BSPII, collagen III, and integrins beta 1 and beta 3). Osteonectin appears to be up-regulated during migration and proliferation, and may mediate the cell-substratum interaction.[14] Osteocalcin is specifically synthesized by differentiated osteoblasts and deposited at the commencement of mineralization.[15,16] Expression of BSPII is considered to be a molecular marker of osteoblastic differentiation.[17] These suggest stimulated proliferation and differentiation of the osteoblastic cells by the DE surface. Although further studies are needed, early establishment of bone-implant integration around the DE surface, as seen by a higher bone-implant contact rate and bone volume in the near zone, may be associated with modulated expression of these genes.

Bone ECM proteins, such as collagen III and BSPII, possess cell-adherent capability. Enhanced production of collagen III and BSPII by the DE surface may mediate cellular adherence to the implant surface through specific cell surface receptors, integrins.[18,19] Further, integrin adhesion and signaling events may mediate the initiation of osteoblastic cellular mineralization.[9] Activation of integrins by the DE implant at the earlier stages may be associated with its rapid increase of bone formation adjacent to the implant surface. Rapid coverage of the implant surface with bone tissue may be a reason why the activity of integrins decreased quickly for the DE implant. In contrast, the sustained expression of integrins for the turned implant may be associated with long-lasting exposure of the implant surface to the surrounding active environment.

Assessment of the surface roughness of implants is important to the point that different measuring systems may provide different values from a sample.[20] The Rp-v, Rrms, and Ra values of the turned implants used in the present study were similar to the values of the commercially pure titanium previously measured by AFM.[21] Interestingly, the present Ra values of the turned and DE implants showed 10% to 20% of values measured by an optical profilometer.[20,22] AFM assesses the surface roughness in a small area with high resolution. Concurrent assessment covering a larger area, such as laser scanning profilometry or interferometry, may provide a more comprehensive evaluation of the surface roughness.

The results of this study indicated that the placement of implants and their surface topography modulated the expression of selected bone matrix–related genes. The modulated osteoblastic phenotype seemed to reflect the bone tissue responses in the near zone. A biomechanical assay using a rat model demonstrated that the DE implants showed greater interfacial shear strength than the turned implant up to week 8 postimplantation.[4] Increased bone-implant contact rate and near zone bone volume associated with increased surface roughness may, in part, explain this biomechanical feature. Further, it should be of future interest to examine whether the disproportionate modulation of the ECM-related genes by implant surface topography also affects the composition and deposition dynamics of bone tissue that may determine the bone-implant contact rate and adhesion strength of integrated tissue.

CONCLUSION

The DE implant showed a greater bone volume than the turned implant in an implant-near zone at week 2 in this experimental model. Also, the DE implant exhibited a greater bone-implant contact rate than the turned implant at weeks 2 and 4. The DE implant evoked an accelerated mRNA expression for osteonectin and osteocalcin compared with the turned implant and an up-regulated expression for BSPII, collagen III, and integrins in initial healing stages up to week 1. These suggest that the gene expression during implant wound healing is regulated at a local level of implant surfaces and that the modulated gene expression may be associated with different histologic bone integration profiles associated with different surface topographies.

ACKNOWLEDGMENT

The authors thank Ms Joyce Shumann (UCLA School of Dentistry) for histologic specimen preparation, and Dr Linda Dubin (UCLA School of Dentistry) and Ms Donna Diamond-Gelinas (UCLA School of Dentistry) for editorial assistance with this manuscript. This study was supported in part by the Academy of Osseointegration, Osseointegration Foundation Research Grant; the Greater New York Academy of Prosthodontics; and 3i Implant Innovations.

REFERENCES

1. LeGeros RZ, Craig RG. Strategies to affect bone remodeling: Osteointegration. J Bone Miner Res 1993;8:S583–S596.
2. Puleo DA, Nanci A. Understanding and controlling the bone-implant interface. Biomaterials 1999;20:2311–2321.
3. Wennerberg A, Albrektsson T, Lausmaa J. Torque and histomorphometric evaluation of c.p. titanium screws blasted with 25- and 75-µm-sized particles of Al_2O_3. J Biomed Mater Res 1996;30:251–260.
4. Ogawa T, Ozawa S, Shih J-H, et al. Biomechanical evaluation of osseous implants having different surface topographies in rats. J Dent Res 2000;79:1857–1863.
5. Howlett CR, Rvans MDM, Walsh WR, Johnson G, Steele JG. Mechanism of initial attachment of cells derived from human bone to commonly used prosthetic materials during cell culture. Biomaterials 1994;15:213–222.
6. Schneider G, Burridge K. Formation of focal adhesions by osteoblasts adhering to different substrata. Exp Cell Res 1994;214:264–269.
7. Martin JY, Schwartz Z, Hummert TW, et al. Effect of titanium surface roughness on proliferation, differentiation, and protein synthesis of human osteoblast-like cells (MG63). J Biomed Mater Res 1995;29:389–401.
8. Lincks J, Boyan BD, Blanchard CR, et al. Response of MG63 osteoblast-like cells to titanium and titanium alloy is dependent on surface roughness and composition. Biomaterials 1998;19:2219–2232.
9. Wong M, Eulenberger J, Schenk R, Hunzider E. Effect of surface topology on the osseointegration of implant materials in trabecular bone. J Biomed Mater Res 1995;29: 1567–1575.
10. Vercaigne S, Wolke JGC, Naert I, Jansen JA. Histomorphometrical and mechanical evaluation of titanium plasma-spray-coated implants placed in the cortical bone of goats. J Biomed Mater Res 1997;41:41–48.
11. Caulier H, van der Waerden JPCM, Wolke JGC, et al. A histological and histomorphometrical evaluation of the application of screw-designed calcium phosphate (Ca-P) coated implants in the cancellous maxillary bone of the goat. J Biomed Mater Res 1997;35:19–30.
12. Garetto LP, Chen J, Andrew J, Roberts WE. Remodeling dynamics of bone supporting rigidly fixed titanium implants: A histomorphometric comparison in four species including humans. Implant Dent 1995;4:235–243.
13. Suzuki K, Aoki K, Ohya K. Effects of surface roughness of titanium implants on bone remodeling activity of femur in rabbits. Bone 1997;21:507–514.
14. Sage H, Vernon RB, Funk SE, Everitt EA, Angello J. SPARC, a secreted protein associated with cellular proliferation, inhibits cell spreading in vitro and exhibits Ca+2-dependent binding to the extracellular matrix. J Cell Biol 1989;109:341–356.
15. Bronckers AL, Gay S, Finkelman RD. Developmental appearance of Gla proteins (osteocalcin) and alkaline phosphatase in tooth germs and bones of the rat. Bone Miner 1987;2:361–373.
16. Camarda AJ, Butler WT, Finkelman RD. Immunocytochemical localization of gamma carboxyglutamic acid–containing proteins and osteocalcin in rat bone and dentin. Calcif Tissue Int 1987;40:349–355.
17. Cooper LF, Harris CT, Bruder SP, Kowalski R, Kadiyala S. Incipient analysis of mesenchymal stem cell–derived osteogenesis. J Dent Res 2001;80:314–320.
18. Morton LF, Peachey AR, Knight G, Farndale RW, Barnes MJ. The platelet reactivity of synthetic peptides based on the collagen III fragment (III)CB4. J Biol Chem 1997;272: 11044–11048.
19. Byzova TV, Kim W, Midura RJ, Plow EF. Activation of integrin alpha (V), beta (3) regulates cell adhesion and migration to bone sialoprotein. Exp Cell Res 2000;254:299–308.
20. Wennerberg A, Albrektsson T. Suggested guidelines for the topographic evaluation of implant sufaces. Int J Oral Maxillofac Implants 2000;15:331–344.
21. Cooper LF, Masuda T, Whitson SW, Yliheikkila P, Felton DA. Formation of mineralizing osteoblast cultures on machined, titanium oxide grit-blasted, and plasma-sprayed titanium surfaces. Int J Oral Maxillofac Implants 1999;14: 37–47.
22. Mustafa K, Lopez BS, Hultenby K, Wennerberg A, Arvidson K. Attachment and proliferation of human oral fibroblasts to titanium surfaces blasted with TiO_2 particles. Clin Oral Impl Res 1998;9:195–207.